View metadata, citation and similar papers at core.ac.uk
brought to you by CORE
provided by Elsevier - Publisher Connector

Available online at www.sciencedirect.com
ScienceDirect
Nuclear and Particle Physics Proceedings 273–275 (2016) 1459–1464
www.elsevier.com/locate/nppp

Branching Fraction and *CP* Asymmetry Measurements in Inclusive $B \to X_s \ell^+ \ell^-$ and $B \to X_s \gamma$ Decays from BABAR

G. Eigen
representing the BABAR collaboration

Department of Physics, University of Bergen, Allegaten 55, N-5007 Bergen, Norway

Abstract

We present an update on total and partial branching fractions and on *CP* asymmetries in the semi-inclusive decay $B \to X_s \ell^+ \ell^-$. Further, we summarize our results on branching fractions and *CP* asymmetries for semi-inclusive and fully-inclusive $B \to X_s \gamma$ decays. We present the first result on the *CP* asymmetry difference of charged and neutral $B \to X_s \gamma$ decays yielding the first constraint on the ratio of Wilson coefficients $Im(C_8^{\rm eff}/C_7^{\rm eff})$.

1. Introduction

The decays $B \to X_{s,d}\gamma$ and $B \to X_{s,d}\ell^+\ell^-$ are flavor-changing neutral current (FCNC) processes that are forbidden in the Standard Model (SM) at tree level. However, they can proceed via penguin loops and box diagrams. Figure 1 shows the lowest-order diagrams for both processes. The effective Hamiltonian factorizes short-distance effects represented by perturbatively-calculable Wilson coefficients (C_i) [1, 2] from long-distance effects specified by four-quark operators (O_i):

$$H_{\rm eff} = \frac{G_F}{4\pi}\Sigma_i V^*_{\rm xb} V_{\rm xs,d} C_i(\mu) O_i. \quad (1)$$

Here, G_F is the Fermi constant, $V^*_{\rm xb}$ and $V_{\rm xs,d}$ are CKM elements ($x = u,\ c,\ t$) and μ is the renormalization scale. The operators have to be calculated using non-perturbative methods, such as the heavy quark expansion [3, 4, 5, 6]. In $B \to X_s\gamma$, the dominant contribution arises from the magnetic dipole operator O_7 with a top quark in the loop. Thus, the branching fraction depends on the Wilson coefficient $C_7^{\rm eff} = -0.304$ (NNLL) [7, 8]. Via operator mixing, the color-magnetic dipole operator O_8 contributes in higher order with $C_8^{\rm eff} = -0.167$ (NNLL) [7, 8]. In $B \to X_s\ell^+\ell^-$, the weak penguin

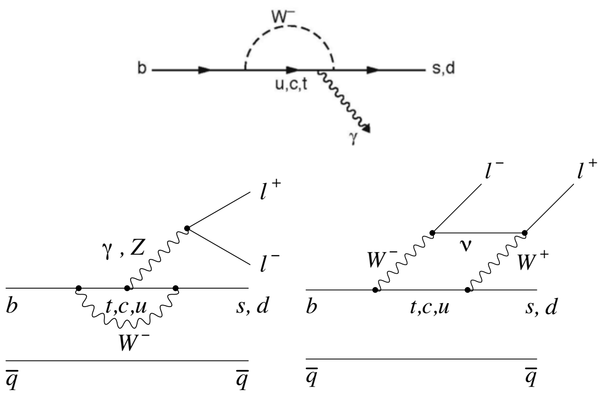

Figure 1: Lowest-order diagrams for $B \to X_{s,d}\gamma$ (top) and $B \to X_{s,d}\ell^+\ell^-$ (bottom).

and box diagrams contribute in addition. The vector part is represented by operator O_9 with Wilson coefficient $C_9^{\rm eff} = 4.211$ (NNLL) [7, 8] while the axial-vector part is specified by operator O_{10} with Wilson coefficient $C_{10}^{\rm eff} = -4.103$ (NNLL) [7, 8]. Again, the top quark in the loop yields the most dominant contribution. New physics adds penguin and box diagrams with new particles modifying the SM values of the Wilson coeffi-

http://dx.doi.org/10.1016/j.nuclphysbps.2015.09.236
2405-6014/© 2016 Published by Elsevier B.V.

cients. In addition, scalar and pseudoscalar couplings may contribute introducing new Wilson coefficients C_S and C_P. Figure 2 shows examples of new physics processes involving a charged Higgs, a chargino and neutralinos [9, 10, 11, 12, 13, 14, 15]. These rare decays probe new physics at a scale of a few TeV.

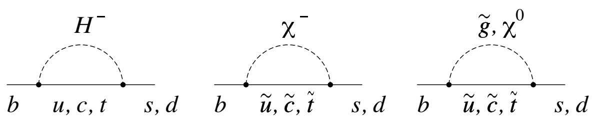

Figure 2: New physics processes with a charged Higgs bosons (left), a chargino plus up-type squarks (middle) and neutralinos plus down-type squarks (right).

2. Study of $B \to X_s \ell^+ \ell^-$

Using a semi-inclusive approach, we have updated the partial and total branching fraction measurements of $B \to X_s \ell^+ \ell^-$ modes with the full *BABAR* data sample of 471×10^6 $B\bar{B}$ events. We also perform the first measurement of direct *CP* asymmetry. For measuring partial and total branching fractions, we reconstruct 20 exclusive final states listed in Table 1. After accounting for K^0_L modes, $K^0_S \to \pi^0\pi^0$ and π^0 Dalitz decays, they represent 70% of the inclusive rate for hadronic masses $m_{X_s} < 1.8$ GeV. Using JETSET fragmentation and theory predictions, we extrapolate for the missing modes and those with $m_{X_s} > 1.8$ GeV. We impose requirements on the beam-energy-substituted mass $m_{ES} = \sqrt{E^2_{CM} - p^{*2}_B} > 5.225$ GeV and on the energy difference -0.1 $(0.05) < \Delta E = E^*_B - E_{CM}/2 < 0.05$ for $X_s\, e^+e^-$ $(X_s\mu\mu)$ modes where E^*_B and p^*_B are B momentum and B energy in the center-of-mass (CM) frame and E_{CM} is the total CM energy. We use no tagging of the $\bar{B}$ decay.

To suppress $e^+e^- \to q\bar{q}$ $(q = u, d, s, c)$ events and $B\bar{B}$ combinatorial background, we define boosted decision trees (BDT) for each q^2 bin in e^+e^- and $\mu^+\mu^-$ separately (see Table 2). From these BDTs, we determine a likelihood ratio (L_R) to separate signal from $q\bar{q}$ and $B\bar{B}$ backgrounds. We veto J/ψ and $\psi(2S)$ mass regions and use them as control samples. Figures 3 and 4 show the m_{ES} and L_R distributions for e^+e^- modes in bin q_5 and for $\mu^+\mu^-$ modes in bin q_1, respectively.

We measure $d\mathcal{B}(B \to X_s\ell^+\ell^-)/dq^2$ in six bins of $q^2 = m^2_{\ell\ell}$ and four bins of m_{X_s} defined in Table 2. We extract the signal in each bin from a two-dimensional fit to m_{ES} and L_R. Figure 5 shows the differential branching faction as a function of q^2 (top) and m_{X_s} (bottom) [16].

Table 1: Exclusive modes used in the semi-inclusive $B \to X_s\ell^+\ell^-$ analysis.

Mode	Mode
$B^0 \to K^0_S\mu^+\mu^-$	$B^+ \to K^+\mu^+\mu^-$
$B^0 \to K^0_S e^+e^-$	$B^+ \to K^+e^+e^-$
$B^0 \to K^{*0}(K^0_S\pi^0)\mu^+\mu^-$	$B^+ \to K^{*+}(K^+\pi^0)\mu^+\mu^-$
$B^0 \to K^{*0}(K^+\pi^-)\mu^+\mu^-$	$B^+ \to K^{*+}(K^0_S\pi^+)\mu^+\mu^-$
$B^0 \to K^{*0}(K^0_S\pi^0)e^+e^-$	$B^+ \to K^{*+}(K^+\pi^0)e^+e^-$
$B^0 \to K^{*0}(K^+\pi^-)e^+e^-$	$B^+ \to K^{*+}(K^0_S\pi^+)e^+e-$
$B^0 \to K^0_S\pi^+\pi^-)\mu^+\mu^-$	$B^+ \to K^0_S\pi^+\pi^0\mu^+\mu^-$
$B^0 \to K^+\pi^-\pi^0\mu^+\mu^-$	$B^+ \to K^+\pi^+\pi^-\mu^+\mu^-$
$B^0 \to K^0_S\pi^+\pi^-)e^+e^-$	$B^+ \to K^0_S\pi^+\pi^0e^+e^-$
$B^0 \to K^+\pi^-\pi^0e^+e^-$	$B^+ \to K^+\pi^+\pi^-e^+e^-$

Table 2: Definition of the q^2 bins.

q^2 bin	q^2 range [GeV^2/c^4]	$m_{\ell\ell}$ range [GeV/c^2]
0	$1.0 < q^2 < 6.0$	$1.00 < m_{\ell\ell} < 2.45$
1	$0.1 < q^2 < 2.0$	$0.32 < m_{\ell\ell} < 1.41$
2	$2.0 < q^2 < 4.3$	$1.41 < m_{\ell\ell} < 2.07$
3	$4.3 < q^2 < 8.1$	$2.07 < m_{\ell\ell} < 2.6$
4	$10.1 < q^2 < 12.9$	$3.18 < m_{\ell\ell} < 3.59$
5	$14.2 < q^2 < (m_B - m^*_K)^2$	$3.77 < m_{\ell\ell} < (m_B - m^*_K)$

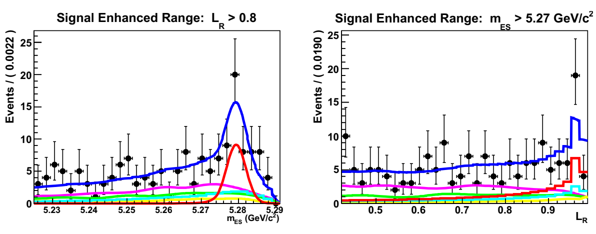

Figure 3: Distributions of m_{ES} (left) and likelihood ratio (right) for $B \to X_s e^+e^-$ in q^2 bin q_5 showing data (points with error bars), the total fit (thick solid blue curves), signal component (red peaking curves), signal cross feed (cyan/lgrey curves), $B\bar{B}$ background (magenta/dark grey smooth curve), $e^+e^- \to q\bar{q}$ background (green/grey curves) and charmonium background (yellow/light grey curves).

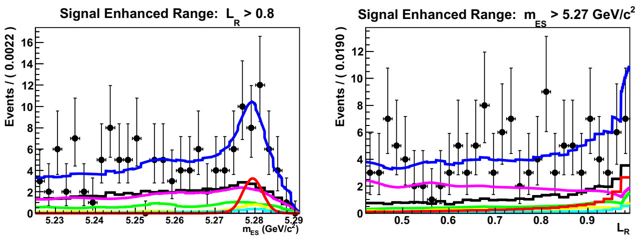

Figure 4: Distributions of m_{ES} (left) and likelihood ratio (right) for $B \to X_s\mu^+\mu^-$ in q^2 bin q_1 showing data (points with error bars), the total fit (thick solid blue curves), signal component (red peaking curves), signal cross feed (cyan/lgrey curves), $B\bar{B}$ background (magenta/dark grey smooth curve), $e^+e^- \to q\bar{q}$ background (green/grey curves) and charmonium background (yellow/light grey curves)

Table 3: The $B \to X_s\ell^+\ell^-$ branching fraction measurements in the low and high q^2 regions [16] in comparison to the SM prediction.

Mode	*BABAR* $[10^{-6}]$	SM $[10^{-6}]$
$q^2[\mathrm{GeV}^2/\mathrm{c}^4]$	$1-6$	$1-6$
$B \to X_s\mu^+\mu^-$	$0.66^{+0.82+0.30}_{-0.76-0.24} \pm 0.07$	1.59 ± 0.11
$B \to X_s e^+e^-$	$1.93^{+0.47+0.21}_{-0.45-0.16} \pm 0.18$	1.64 ± 0.11
$B \to X_s\ell^+\ell^-$	$1.60^{+0.41+0.17}_{-0.39-0.13} \pm 0.07$	
$q^2[\mathrm{GeV}^2/\mathrm{c}^4]$	> 14.2	> 14.2
$B \to X_s\mu^+\mu^-$	$0.60^{+0.31+0.05}_{-0.29-0.04} \pm 0.00$	$0.25^{+0.07}_{-0.06}$
$B \to X_s e^+e^-$	$0.56^{+0.19+0.03}_{-0.18-0.03} \pm 0.00$	
$B \to X_s\ell^+\ell^-$	$0.57^{+0.16+0.03}_{-0.15-0.02} \pm 0.00$	

Table 3 summarizes the differential branching fractions in the low and high q^2 regions in comparison to the SM predictions [17, 18, 19, 18, 20, 21, 22, 23, 24, 25, 26, 27]. In both regions of q^2, the differential branching fraction is in good agreement with the SM prediction. These results supersede the previous *BABAR* measurements [28] and are in good agreement with the Belle results [29].

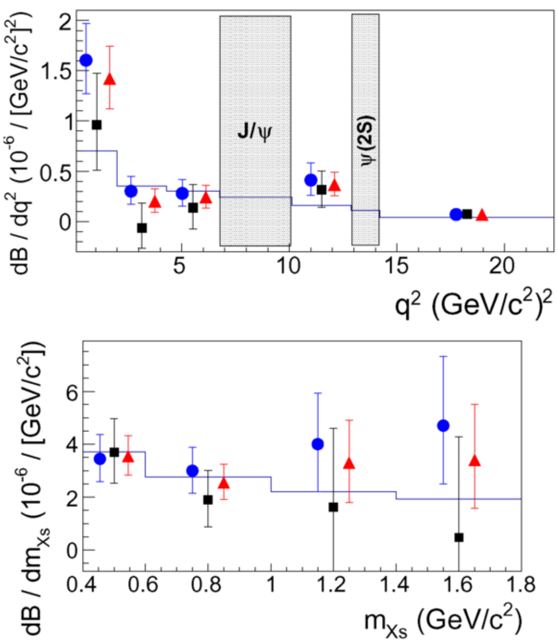

Figure 5: Differential branching fraction of $B \to X_s e^+e^-$ (blue points), $B \to X_s\mu^+\mu^-$ (black squares), and $B \to X_s\ell^+\ell^-$ (red triangles) versus q^2 (top) and versus m_{X_s} (bottom) in comparison to the SM prediction (histogram). The grey-shaded bands show the J/ψ and $\psi(2S)$ vetoed regions.

The direct *CP* asymmetry is defined by:

$$\mathcal{A}_{CP} = \frac{\mathcal{B}(\bar{B} \to \bar{X}_s\ell^+\ell^-) - \mathcal{B}(B \to X_s\ell^+\ell^-)}{\mathcal{B}(\bar{B} \to \bar{X}_s\ell^+\ell^-) + \mathcal{B}(B \to X_s\ell^+\ell^-)}. \quad (2)$$

We use 14 self-tagging modes consisting of all B^+ modes and the B^0 modes with decays to a K^+ listed in Table 1 to measure $\mathcal{A}_{CP}(B \to X_s\ell^+\ell^-)$ in five q^2 bins. Note that we have combined bins q_4 and q_5 due to low statistics. Figure 6 shows the *CP* asymmetry as a function of q^2. The SM prediction of the *CP* asymmetry in the entire q^2 region is close to zero [30, 31, 32, 8]. In new physics models, however, $\mathcal{A}_{CP}$ may be significantly enhanced [11, 33]. In the full range of q^2 we measure $\mathcal{A}_{CP} = 0.04 \pm 0.11 \pm 0.01$ [16], which is in good agreement with the SM prediction. The *CP* asymmetries in the five q^2 bins are also consistent with zero.

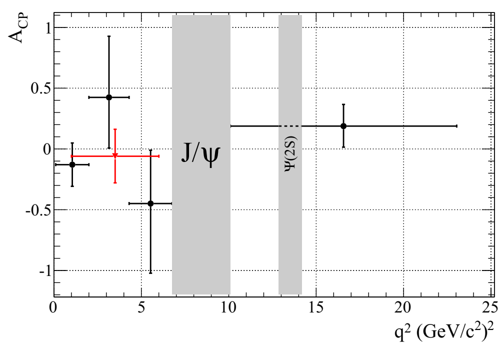

Figure 6: The *CP* asymmetry as a function of q^2. The grey-shaded bands show the J/ψ and $\psi(2S)$ vetoed regions.

3. Study of $B \to X_s\gamma$

In the SM, the $B \to X_s\gamma$ branching fraction is calculated in next-to-next leading order (4 loops) yielding

$$\mathcal{B}(B \to X_s\gamma) = (3.15 \pm 0.23) \times 10^{-4} \tag{3}$$

for photon energies $E_\gamma > 1.6$ GeV [34, 35].

To extract the $B \to X_s\gamma$ signal experimentally from $e^+e^- \to B\bar{B}$ and $e^+e^- \to q\bar{q}$ backgrounds, we use two very different strategies. The first strategy consists of a semi-inclusive approach in which we sum over 38 exclusive $B \to X_s\gamma$ final states with $1K^\pm (\leq 1K_S^0)$ or 3 $K^\pm$, $\leq 4\pi(\leq 2\pi^0)$, and $\leq 1\eta$. We use no tagging of the other B meson. We need to model the missing modes. Due to large backgrounds, we select events with a minimum photon energy of $E_\gamma > 1.9$ GeV and then extrapolate the branching fraction to photon energies $E_\gamma > 1.6$ GeV. With this approach, we measure the branching fraction, *CP* asymmetry and the difference in *CP* asymmetries between charged and neutral B decays using 471×10^6 $B\bar{B}$ events [36].

The second strategy is a fully inclusive approach. To suppress backgrounds from $B\bar{B}$ and $q\bar{q}$ decays, we impose stringent constraints on isolated photons to remove clusters that may have originated from π^0 and η decays. We use a semileptonic tag of the other B meson and require a minimum photon energy of $E_\gamma > 1.8$ GeV but impose no requirements on the hadronic mass system. Using 383×10^6 $B\bar{B}$ events, we measure the $B \to X_s\gamma$ branching fraction measurement and the *CP* asymmetry for $B \to X_{s+d}\gamma$ [37, 38].

Table 4 summarizes our $B \to X_s\gamma$ branching fraction measurements of the semi-inclusive and fully inclusive methods [36, 37, 38]. Figure 7 shows the *BABAR* results extrapolated to a minimum photon energy of 1.6 GeV in comparison to results from Belle [40, 41, 42], CLEO [43] and the SM prediction [34, 35]. Our results are in good agreement with those of the other experiments as well as the SM prediction.

For the semi-inclusive method, the direct *CP* asymmetry is defined by:

$$\mathcal{A}_{CP}(X_s\gamma) = \frac{\mathcal{B}(\bar{B} \to \bar{X}_s\gamma) - \mathcal{B}(B \to X_s\gamma)}{\mathcal{B}(\bar{B} \to \bar{X}_s\gamma) + \mathcal{B}(B \to X_s\gamma)}. \tag{4}$$

The SM prediction yields $-0.6\% < \mathcal{A}_{CP}(B \to X_s\gamma) < 2.8\%$ [45, 46]. Using 16 self-tagging exclusive modes and 471×10^6 $B\bar{B}$ events, we measure $\mathcal{A}_{CP}(B \to X_s\gamma) = (1.7 \pm 1.9_{stat} \pm 1.0_{sys})\%$ [47]. This supersedes the old *BABAR* measurement [48].We further measures the *CP* asymmetry difference between charged and neutral B decays:

$$\Delta\mathcal{A}_{CP} = \mathcal{A}_{CP}(B^+ \to X_s^+\gamma) - \mathcal{A}_{CP}(B^0 \to X_s^0\gamma), \tag{5}$$

Table 4: Our measurements of $\mathcal{B}(B \to X_s\gamma)$ from the semi-inclusive [36] and fully-inclusive [37] analyses and their extrapolations to $E_\gamma > 1.6$ GeV. The first uncertainty is statistical, the second is systematic and the third is from model dependence and extrapolation to 1.6 GeV.

method	$E_\gamma >$	$\mathcal{B}(B \to X_s\gamma)$ $[10^{-4}]$
semi-	1.9 GeV	$3.29 \pm 0.19 \pm 0.48$
exclusive	1.6 GeV	$3.52 \pm 0.20 \pm 0.51 \pm 0.04$
inclusive	1.8 GeV	$3.21 \pm 0.15 \pm 0.29 \pm 0.08$
	1.6 GeV	$3.31 \pm 0.16 \pm 0.30 \pm 0.10$

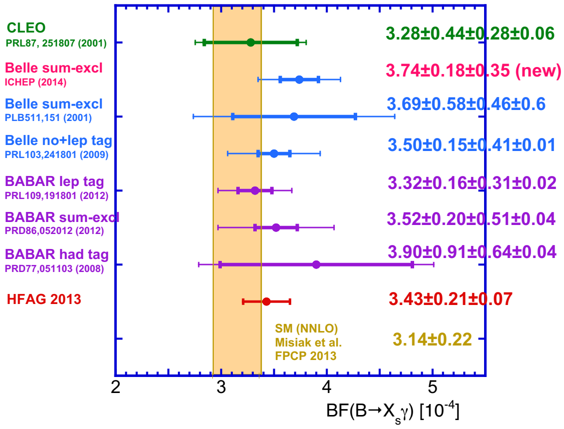

Figure 7: Summary of $\mathcal{B}(B \to X_s\gamma)$ measurements from BABAR [36, 37, 38, 39], Belle [40, 41, 42], CLEO [43] and the HFAG average [44] in comparison to the SM prediction [34, 35] after extrapolation to $E_\gamma^* > 1.6$ GeV.

which depends on the Wilson coefficients C_7^{eff} and C_8^{eff}:

$$\Delta\mathcal{A}_{CP} = 4\pi^2\alpha_s \frac{\bar{\Lambda}_{78}}{m_b} Im\frac{C_8^{\mathrm{eff}}}{C_7^{\mathrm{eff}}} \simeq 0.12 \frac{\bar{\Lambda}_{78}}{100\ \mathrm{MeV}} Im\frac{C_8^{\mathrm{eff}}}{C_7^{\mathrm{eff}}} \tag{6}$$

where the scale parameter $\bar{\Lambda}_{78}$ is constrained by $17\ \mathrm{MeV} < \bar{\Lambda}_{78} < 190\ \mathrm{MeV}$. In the SM, C_7^{eff} and C_8^{eff} are real so that $\Delta\mathcal{A}_{CP}$ vanishes. However in new physics models, these Wilson coefficients may have imaginary parts yielding a non-vanishing $\Delta\mathcal{A}_{CP}$.

From a simultaneous fit to charged and neutral B decays, we measure $\Delta\mathcal{A}_{CP}(B \to X_s\gamma) = (5.0 \pm 3.9_{stat} \pm 1.5_{sys})\%$ from which we set an upper and lower limit at 90% *CL* on $Im(C_8^{\mathrm{eff}}/C_7^{\mathrm{eff}})$ [47]:

$$-1.64 < Im\frac{C_8^{\mathrm{eff}}}{C_7^{\mathrm{eff}}} < 6.52\ \mathit{at}\ 90\%\ CL. \tag{7}$$

This is the first $\Delta\mathcal{A}_{CP}$ measurements and the first constraint on $Im(C_8^{\mathrm{eff}}/C_7^{\mathrm{eff}})$. Figure 8 (top) shows the $\Delta\chi^2$ of the fit as a function of $Im(C_8^{\rm eff}/C_7^{\rm eff})$. The shape of $\Delta\chi^2$ as a function of $\mathcal{I}m(C_8^{\rm eff}/C_7^{\rm eff})$ is not parabolic indicating that the likelihood has a non-Gaussian shape. The reason is that $\Delta\chi^2$ is determined from all possible values of $\bar{\Lambda}_{78}$. In the region $\sim 0.2 < \mathcal{I}m(C_8^{\rm eff}/C_7^{\rm eff}) <\sim 2.6$ a change in $\mathcal{I}m(C_8^{\rm eff}/C_7^{\rm eff})$ $\Delta\chi^2$ can be compensated by a change in $\bar{\Lambda}_{78}$ leaving $\Delta\chi^2$ unchanged. For positive values larger (smaller) than 2.6 (0.2), $\Delta\chi^2$ increases slowly (rapidly), since $\bar{\Lambda}_{78}$ remains nearly constant at the minimum value (increases rapidly). For negative $\mathcal{I}m(C_8^{\rm eff}/C_7^{\rm eff})$ values, $\bar{\Lambda}_{78}$ starts to decrease again, which leads to a change in the $\Delta\chi^2$ shape. Figure 8 (bottom) shows $\bar{\Lambda}_{78}$ as a function of $Im(C_8^{\rm eff}/C_7^{\rm eff})$.

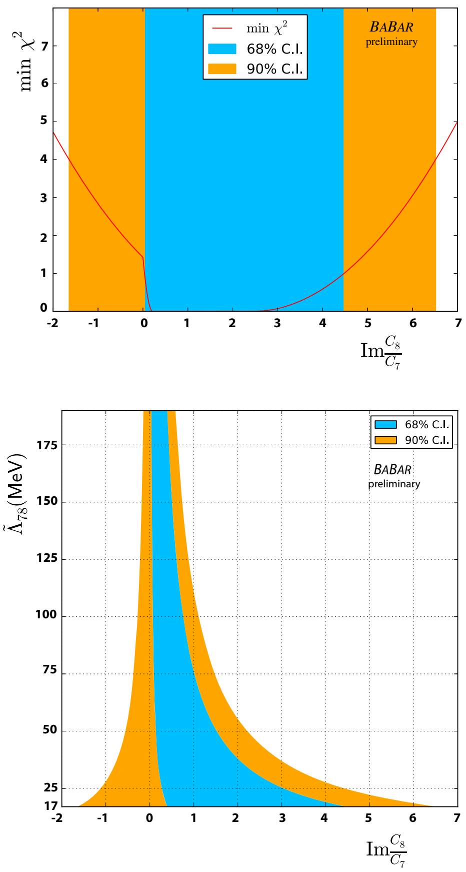

Figure 8: The $\Delta\chi^2$ function versus $\mathcal{I}m(C_8^{\rm eff}/C_7^{\rm eff})$ (top) and the dependence of $\bar{\Lambda}_{78}$ on $\mathcal{I}m(C_8^{\rm eff}/C_7^{\rm eff})$ (bottom). The blue dark-shaded (orange light-shaded) regions show the 68% (90%) CL intervals.

In the fully-inclusive analysis, the $B \to X_d$ decay cannot be separated from the $B \to X_s$ decay and we measure:

$$\mathcal{A}_{CP}(X_{s+d}\gamma) = \frac{\mathcal{B}(\bar{B} \to \bar{X}_{s+d}\gamma) - \mathcal{B}(B \to X_{s+d}\gamma)}{\mathcal{B}(\bar{B} \to \bar{X}_{s+d}\gamma) + \mathcal{B}(B \to X_{s+d}\gamma)}. \quad (8)$$

In the SM, $\mathcal{A}_{CP}(B \to X_{s+d}\gamma)$ is zero [49]. From the charge of the B and $\bar{B}$, we determine the CP asymmetry. Using 383×10^6 $B\bar{B}$ events, we measure $\mathcal{A}_{CP}(B \to X_{s+d}\gamma) = (5.7 \pm 6.0 \pm 1.8)\%$, which is consistent with the SM prediction [49]. Figure 9 shows a summary of all CP asymmetry measurements in comparison to the SM predictions.

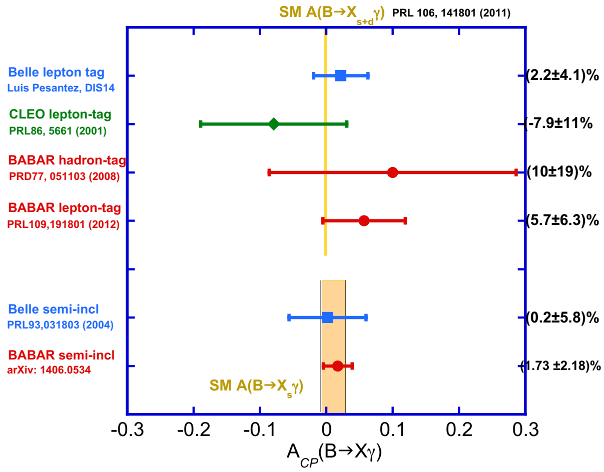

Figure 9: Summary of $\mathcal{A}_{CP}$ measurements for $B \to X_s\gamma$ from semi-inclusive analyses (*BABAR* [47], Belle [50]) and for $B \to X_{s+d}\gamma$ from fully inclusive analyses (*BABAR* [37, 38, 39], CLEO [51]), Belle [52] and the HFAG average [44] in comparison to the SM prediction for $B \to X_s\gamma$ [45, 46, 49].

4. Conclusion

We performed the first $\mathcal{A}_{CP}$ measurement in five q^2 bins in semi-inclusive $B \to X_s\ell^+\ell^-$ decays and updated the differential branching fraction. The $B \to X_s\ell^+\ell^-$ partial branching fractions and CP asymmetries are in good agreement with the SM predictions. Our $\mathcal{A}_{CP}$ measurement in the semi-inclusive $B \to X_s\gamma$ decay is the most precise CP asymmetry measurement. The $\Delta\mathcal{A}_{CP}(B \to X_s\gamma)$ result yields first constraint on $Im(C_8^{\rm e}/C_7^{\rm e})$. The $B \to X_s\gamma$ branching fractions and CP asymmetries are both in good agreement with the SM predictions. New progress on these inclusive decays will come from Belle II. For the $B \to X_s\gamma$ and $B \to X_s\ell^+\ell^-$ semi-inclusive decays, we expect precision measurements. For the inclusive $B \to X_s\gamma$ and $B \to X_s\ell^+\ell^-$ decays, we expect new possibilities by tagging the other $\bar{B}$ meson via full B reconstruction.

5. Acknowledgments

This work was supported by the Norwegian Research Council. I would like to thank members of the *BABAR* collaboration for giving me the opportunity to present these results. In particular, I would like to thank Doug Roberts, Liang Sun and David Hitlin for their fruitful suggestions.

References

[1] K. G. Wilson, Phys. Rev. **179**, 1499 (1969).
[2] K. G. Wilson and J. B. Kogut, Phys. Rept. **12**, 75 (1974).
[3] N. Isgur, D. Scora, B. Grinstein and M. B. Wise, Phys. Rev. D **39**, 799 (1989).
[4] N. Isgur and M. B. Wise, Phys. Lett. B **232**, 113 (1989).
[5] H. Georgi, Phys. Lett. B **240**, 447 (1990).
[6] B. Grinstein and D. Pirjol, Phys. Rev. D **70**, 114005 (2004) [hep-ph/0404250].
[7] G. Buchalla, A. J. Buras and M. E. Lautenbacher, Rev. Mod. Phys. **68**, 1125 (1996) [hep-ph/9512380].
[8] W. Altmannshofer, P. Ball, A. Bharucha, A. J. Buras, D. M. Straub and M. Wick, JHEP **0901**, 019 (2009) [arXiv:0811.1214 [hep-ph]].
[9] A. Ali, E. Lunghi, C. Greub and G. Hiller, Phys. Rev. D **66**, 034002 (2002) [hep-ph/0112300].
[10] K. S. M. Lee and F. J. Tackmann, Phys. Rev. D **79**, 114021 (2009) [arXiv:0812.0001 [hep-ph]].
[11] A. Soni, A. K. Alok, A. Giri, R. Mohanta and S. Nandi, Phys. Rev. D **82**, 033009 (2010) [arXiv:1002.0595 [hep-ph]].
[12] S. Oh and J. Tandean, Phys. Rev. D **83**, 095006 (2011) [arXiv:1102.1680 [hep-ph]].
[13] S. Descotes-Genon, D. Ghosh, J. Matias and M. Ramon, JHEP **1106**, 099 (2011) [arXiv:1104.3342 [hep-ph]].
[14] W. Altmannshofer, P. Paradisi and D. M. Straub, JHEP **1204**, 008 (2012) [arXiv:1111.1257 [hep-ph]].
[15] N. Kosnik, Phys. Rev. D **86**, 055004 (2012) [arXiv:1206.2970 [hep-ph]].
[16] J. P. Lees *et al.* [BaBar Collaboration], Phys. Rev. Lett. **112**, 211802 (2014) [arXiv:1312.5364 [hep-ex]].
[17] H. H. Asatryan, H. M. Asatrian, C. Greub and M. Walker, Phys. Rev. D **65**, 074004 (2002) [hep-ph/0109140].
[18] H. H. Asatryan, H. M. Asatrian, C. Greub and M. Walker, Phys. Rev. D **66**, 034009 (2002) [hep-ph/0204341].
[19] A. Ghinculov, T. Hurth, G. Isidori and Y. P. Yao, Nucl. Phys. B **648**, 254 (2003) [hep-ph/0208088].
[20] P. Gambino, M. Gorbahn and U. Haisch, Nucl. Phys. B **673**, 238 (2003) [hep-ph/0306079].
[21] A. Ghinculov, T. Hurth, G. Isidori and Y. P. Yao, Eur. Phys. J. C **33**, S288 (2004) [hep-ph/0310187].
[22] C. Bobeth, P. Gambino, M. Gorbahn and U. Haisch, JHEP **0404**, 071 (2004) [hep-ph/0312090].
[23] A. Ghinculov, T. Hurth, G. Isidori and Y. P. Yao, Nucl. Phys. B **685**, 351 (2004) [hep-ph/0312128].
[24] C. Greub, V. Pilipp and C. Schupbach, JHEP **0812**, 040 (2008) [arXiv:0810.4077 [hep-ph]].
[25] T. Huber, T. Hurth and E. Lunghi, Nucl. Phys. B **802**, 40 (2008) [arXiv:0712.3009 [hep-ph]].
[26] T. Huber, E. Lunghi, M. Misiak and D. Wyler, Nucl. Phys. B **740**, 105 (2006) [hep-ph/0512066].
[27] M. Beneke, G. Buchalla, M. Neubert and C. T. Sachrajda, Eur. Phys. J. C **61**, 439 (2009) [arXiv:0902.4446 [hep-ph]].
[28] B. Aubert *et al.* [BaBar Collaboration], Phys. Rev. Lett. **93**, 081802 (2004) [hep-ex/0404006].
[29] M. Iwasaki *et al.* [Belle Collaboration], Phys. Rev. D **72**, 092005 (2005) [hep-ex/0503044].
[30] D. S. Du and M. Z. Yang, Phys. Rev. D **54**, 882 (1996) [hep-ph/9510267].
[31] A. Ali and G. Hiller, Eur. Phys. J. C **8**, 619 (1999) [hep-ph/9812267].
[32] C. Bobeth, G. Hiller and G. Piranishvili, JHEP **0807**, 106 (2008) [arXiv:0805.2525 [hep-ph]].
[33] A. K. Alok, A. Dighe and S. Ray, Phys. Rev. D **79**, 034017 (2009) [arXiv:0811.1186 [hep-ph]].
[34] M. Misiak, H. M. Asatrian, K. Bieri, M. Czakon, A. Czarnecki, T. Ewerth, A. Ferroglia and P. Gambino *et al.*, Phys. Rev. Lett. **98**, 022002 (2007) [hep-ph/0609232].
[35] M. Misiak and M. Steinhauser, Nucl. Phys. B **764**, 62 (2007) [hep-ph/0609241].
[36] J. P. Lees *et al.* [BaBar Collaboration], Phys. Rev. D **86**, 052012 (2012) [arXiv:1207.2520 [hep-ex]].
[37] J. P. Lees *et al.* [BaBar Collaboration], Phys. Rev. Lett. **109**, 191801 (2012) [arXiv:1207.2690 [hep-ex]].
[38] J. P. Lees *et al.* [BaBar Collaboration], Phys. Rev. D **86**, 112008 (2012) [arXiv:1207.5772 [hep-ex]].
[39] B. Aubert *et al.* [BaBar Collaboration], Phys. Rev. D **77**, 051103 (2008) [arXiv:0711.4889 [hep-ex]].
[40] K. Abe *et al.* [Belle Collaboration], Phys. Lett. B **511**, 151 (2001) [hep-ex/0103042].
[41] A. Limosani *et al.* [Belle Collaboration], Phys. Rev. Lett. **103**, 241801 (2009) [arXiv:0907.1384 [hep-ex]].
[42] T. Saito *et al.* [Belle Collaboration], Talk at Moriond Electroweak 2014.
[43] S. Chen *et al.* [CLEO Collaboration], Phys. Rev. Lett. **87**, 251807 (2001) [hep-ex/0108032].
[44] D. Asner *et al.* [Heavy Flavor Averaging Group Collaboration], arXiv:1010.1589 [hep-ex].
[45] A. L. Kagan and M. Neubert, Phys. Rev. D **58**, 094012 (1998) [hep-ph/9803368].
[46] M. Benzke, S. J. Lee, M. Neubert and G. Paz, Phys. Rev. Lett. **106**, 141801 (2011) [arXiv:1012.3167 [hep-ph]].
[47] J. P. Lees *et al.* [BaBar Collaboration], arXiv:1406.0534 [hep-ex].
[48] B. Aubert *et al.* [BaBar Collaboration], Phys. Rev. Lett. **101**, 171804 (2008) [arXiv:0805.4796 [hep-ex]].
[49] T. Hurth, E. Lunghi and W. Porod, Nucl. Phys. B **704**, 56 (2005) [hep-ph/0312260].
[50] S. Nishida *et al.* [Belle Collaboration], Phys. Rev. Lett. **93**, 031803 (2004) [hep-ex/0308038].
[51] T. E. Coan *et al.* [CLEO Collaboration], Phys. Rev. Lett. **86**, 5661 (2001) [hep-ex/0010075].
[52] L. Pesantez *et al.* [Belle Collaboration], talk at DIS14, arXiv:1406.6356 [hep-ex].